Complete set of deuteron analyzing powers for dp elastic scattering at 250–294 MeV/nucleon and the three-nucleon force

K. Sekiguchi,[1,*] Y. Wada,[1] J. Miyazaki,[1] H. Witała,[2] M. Dozono,[3] U. Gebauer,[1] J. Golak,[2] H. Kamada,[4] S. Kawase,[5] Y. Kubota,[5] C. S. Lee,[5] Y. Maeda,[6] T. Mashiko,[1] K. Miki,[7] A. Nogga,[8] H. Okamura,[7] T. Saito,[6] H. Sakai,[3] S. Sakaguchi,[9] N. Sakamoto,[3] M. Sasano,[3] Y. Shimizu,[3] R. Skibiński,[2] H. Suzuki,[3] T. Taguchi,[1] K. Takahashi,[1] T. L. Tang,[5] T. Uesaka,[3] T. Wakasa,[9] and K. Yako[5]

[1]*Department of Physics, Tohoku University, Sendai, 980-8578, Japan*
[2]*Institute of Physics, Jagiellonian University, PL-30059 Cracow, Poland*
[3]*RIKEN Nishina Center, Wako, 351-0198, Japan*
[4]*Department of Physics, Kyushu Institute of Technology, Kitakyushu 804-8550, Japan*
[5]*Center for Nuclear Study, University of Tokyo, Tokyo, 113-0033, Japan*
[6]*Faculty of Engineering, University of Miyazaki, Miyazaki, 889-2192, Japan*
[7]*Research Center for Nuclear Physics, Osaka University, Ibaraki, Osaka, 567-0047, Japan*
[8]*Institut für Kernphysik, Institute for Advanced Simulation and Jülich Center for Hadron Physics, Forschungszentrum Jülich D-52428 Jülich, Germany*
[9]*Department of Physics, Kyushu University, Fukuoka, 812-8581, Japan*

(Received 12 April 2014; published 24 June 2014)

A complete high-precision set of deuteron analyzing powers for elastic deuteron-proton (dp) scattering at 250 and 294 MeV/nucleon has been measured. These data and previously existing data sets for the cross section at similar energies are compared to the results of three-nucleon Faddeev calculations based on modern nucleon-nucleon (NN) potentials alone or combined with two models of three-nucleon forces: the Tucson-Melbourne 99 and Urbana IX. Large discrepancies between pure NN theory and data, which are not resolved by the current three-nucleon forces, were found at c.m. backward angles $\theta_{\mathrm{c.m.}} \gtrsim 120^\circ$ for all the deuteron analyzing powers and the cross section. Because only small relativistic effects were found for the deuteron analyzing powers and the cross section, the inclusion of short-range components of the three-nucleon force is probably required to get a better description of the data.

DOI: 10.1103/PhysRevC.89.064007 PACS number(s): 21.30.−x, 21.45.−v, 24.10.−i, 24.70.+s

I. INTRODUCTION

High-precision nucleon-nucleon (NN) potentials such as AV18 [1], CD Bonn [2], and Nijmegen I, II, and 93 [3] provide a good description of the NN data up to ∼350 MeV. When these forces are used to predict binding energies of three nucleon ($3N$) systems, however, they underestimate the experimental bindings of ^{3}H and ^{3}He. The underbinding of ^{3}H and ^{3}He can be explained by adding a three-nucleon force ($3N$F), mostly based on 2π exchange, acting between three nucleons [4–6]. The importance of $3N$Fs has been further supported by the binding energies of light mass nuclei and by the empirical saturation point of symmetric nuclear matter. *Ab initio* microscopic calculations of light mass nuclei, such as Green's function Monte Carlo [7] and no-core shell model calculations [8], highlight the necessity of including $3N$Fs to explain the binding energies and low-lying levels of these nuclei. As for the density of symmetric nuclear matter, it has been reported that all NN potentials provide saturation at too high density, and a short-range repulsive $3N$F is one possibility to shift the theoretical results to the empirical point [9]. In the past decade, low energy scattering, binding energies of light [10], medium mass nuclei [11,12], and nuclear matter [13] have been extensively studied also in the framework of chiral effective field theory (χEFT). In all these investigations, it became evident that $3N$Fs are taken as one key element to understand various nuclear phenomena. Therefore, they should be investigated in a wide momentum region to understand their properties in detail.

Nucleon-deuteron (Nd) scattering, for which a rigorous formulation in terms of Faddeev equations exists and exact solutions of these equations for any dynamical input can be obtained, offers a good opportunity to study the dynamical aspects of $3N$Fs since this process provides not only cross sections but also a variety of spin observables at different incident nucleon energies. The importance of $3N$Fs in Nd elastic scattering was shown for the first time in Ref. [14]. Clear signals from $3N$Fs were found around the cross-section minimum occurring at c.m. angle $\theta_{c.m.} \approx 120^\circ$ for incident energies above 60 MeV/nucleon. Since then experimental studies of proton-deuteron (pd) and neutron-deuteron (nd) elastic scattering at intermediate energies have been performed extensively and have provided precise data for the cross section [15–21] and spin observables [15–19,21–27]. Large discrepancies between data and rigorous Faddeev calculations with modern NN forces alone have been reported, which are particularly significant in the angular region of the cross-section minimum and at incident nucleon energies above about 60 MeV/nucleon. In the case of the cross section, a large part of the discrepancies is removed by combining the NN forces with a $3N$F, such as the Tucson-Melbourne (TM99) [28] or

*kimiko@lambda.phys.tohoku.ac.jp

Urbana IX [29]. Those results can be taken as clear signatures for $3N$F effects in Nd elastic scattering and the data form a solid basis to test new theoretical models. The theoretical predictions with 3NFs included still have difficulties in reproducing data for some spin observables.

Studies of three nucleon scattering at higher energies are motivated by the fact that the theoretical predictions reveal large effects of $3N$Fs at higher incident energies. In Refs. [18,21], precise data for the cross section and the nucleon analyzing powers at 250 MeV/nucleon in pd and nd elastic scattering were reported. Recently all deuteron analyzing powers (iT_{11}, T_{20}, T_{21}, and T_{22}) at 250 MeV/nucleon have been measured at RIKEN RI Beam Factory (RIBF) [27]. Contrary to the results obtained at lower energies, the discrepancies in the cross section are only partially removed by incorporating $3N$Fs and large discrepancies of $\approx$40 % still remain at backward angles $\theta_{\mathrm{c.m.}} \gtrsim 120^\circ$. All measured spin observables behave similarly to the cross section; i.e., the data at the backward angles $\theta_{\mathrm{c.m.}} \gtrsim 120^\circ$ are not reproduced by the calculations even adding the current $3N$Fs, while the data at the forward angles are mostly explained by the calculations with the current $3N$Fs.

The results obtained at 250 MeV/nucleon indicate that some significant dynamical components are missing in the calculations in the regions of higher momentum transfer. In order to obtain consistent understanding of the dynamics of nuclear forces, high-precision data covering wide energies are needed. So far, however, few precise data exist around 200–300 MeV/nucleon. Therefore, following the first experiment with polarized deuteron beams at RIBF [27], we extended our measurements to 294 MeV/nucleon, providing a high-precision data set for all deuteron analyzing powers in a wide angular range $\theta_{\mathrm{c.m.}} = 35$–$163^\circ$.

In this paper we present the measured complete set of deuteron analyzing powers at 250 and 294 MeV/nucleon and compare them with the Faddeev calculations based on the NN forces alone and combined with the TM99 or Urbana IX $3N$Fs. In this way we show how the state-of-the-art calculations describe the experimental data. In addition, relativistic effects that could become significant at higher energies are studied by the relativistic Faddeev calculations with the TM99 $3N$F included, as reported in Ref. [30].

Our paper is organized as follows. In Sec. II we present the details of the experimental arrangement. Section III deals with the data analysis and presents the experimental results. In Sec. IV we review the basics of the theoretical $3N$ scattering formalism and give a short description of the dynamical input used in the study. The experimental results are compared with the theoretical predictions in Sec. V. Section VI presents a summary and conclusions.

II. EXPERIMENTAL PROCEDURE

A. Polarized deuteron beams

All deuteron analyzing powers for elastic dp scattering were measured with the BigDpol system at RIBF. A schematic view of the experimental setup is shown in Fig. 1.

The vector and tensor polarized deuteron beam was provided by the polarized ion source [31] and was accelerated by the AVF, RRC, and SRC through the Intermediate-stage Ring Cyclotron (IRC) bypass transport beam line [32]. The deuteron polarization axis was rotated by a spin rotation Wien filter system [33] prior to acceleration. That axis was normal to the scattering plane when measuring the analyzing

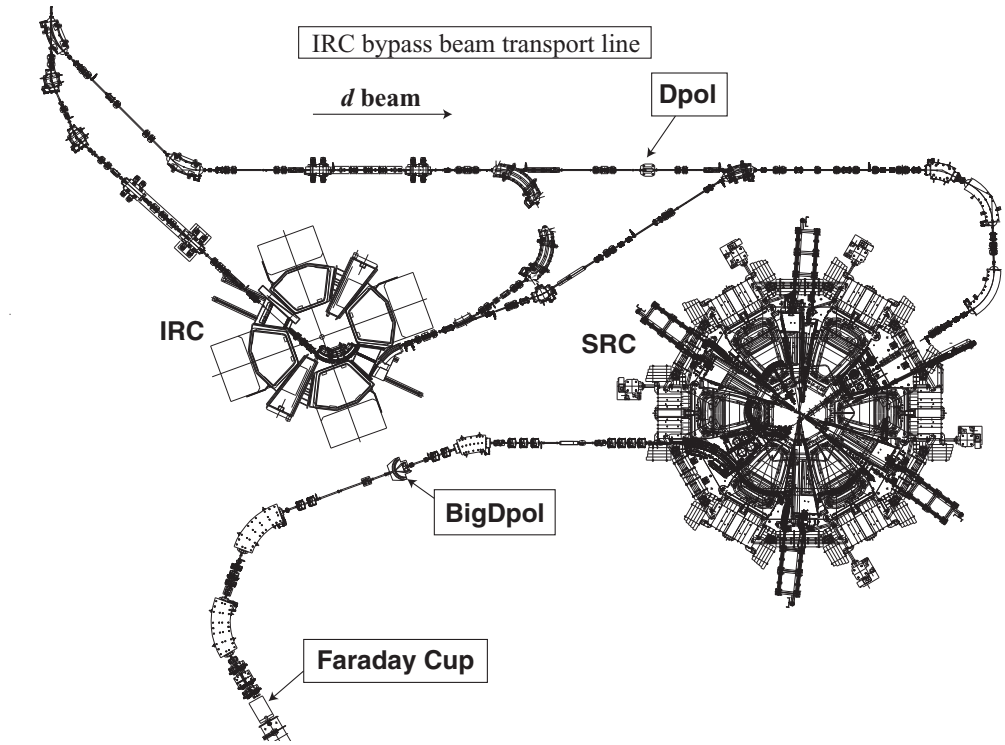

FIG. 1. Schematic view of the experimental setup.

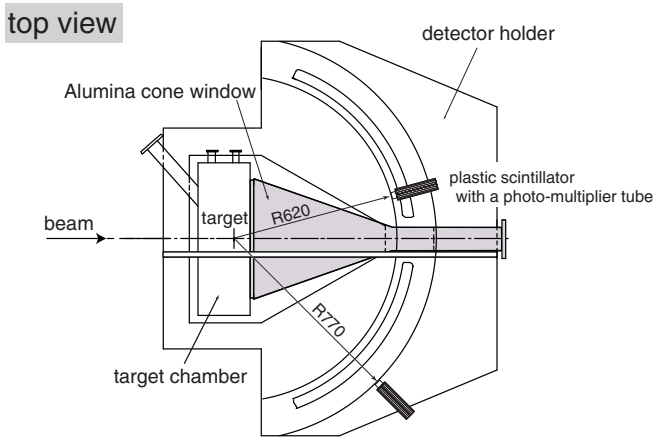

FIG. 2. (Color online) Top view of the BigDpol.

powers iT_{11}, T_{20}, and T_{22}. For the T_{21} measurement the spin symmetry axis was rotated in the reaction plane and aligned at an angle $\beta = 38.0^\circ \pm 0.51^\circ$ ($45.0^\circ \pm 1.2^\circ$) with respect to the beam direction at 250 MeV/nucleon (294 MeV/nucleon). The beam polarizations were monitored continuously with a beam line polarimeter Dpol using elastic dp scattering at 90 (100) MeV/nucleon [17,34]. In the present measurement typical values of the beam polarizations were 80% of the theoretical maximum values.

B. Detector arrangement

The detection setup BigDpol was installed at the extraction beam line of the SRC (see Fig. 1). The BigDpol consists of the target chamber, the aluminum cone window of 2 mm thickness, and the detector holders (see Fig. 2). The four pairs of plastic scintillation counters (BICRON 408) coupled with photomultiplier tubes (Hamamatsu 7415) are mounted in two independent planes perpendicular to each other. The opening angle of the BigDpol is 7.5–70°, which corresponds to the scattering angles $\theta_{\text{c.m.}} = 35$–$163^\circ$ in the center-of-mass system for elastic dp scattering.

The deuteron beams bombarded a polyethylene (CH_2) target with a thickness of 330 mg/cm^2 placed in the scattering chamber. The scattered deuterons and recoil protons were detected in a kinematical coincidence condition by each pair of the detectors. The solid angles were determined by the proton detectors with the angular spread $\Delta\theta_{\text{lab.}} = \pm 1^\circ$. The deuteron

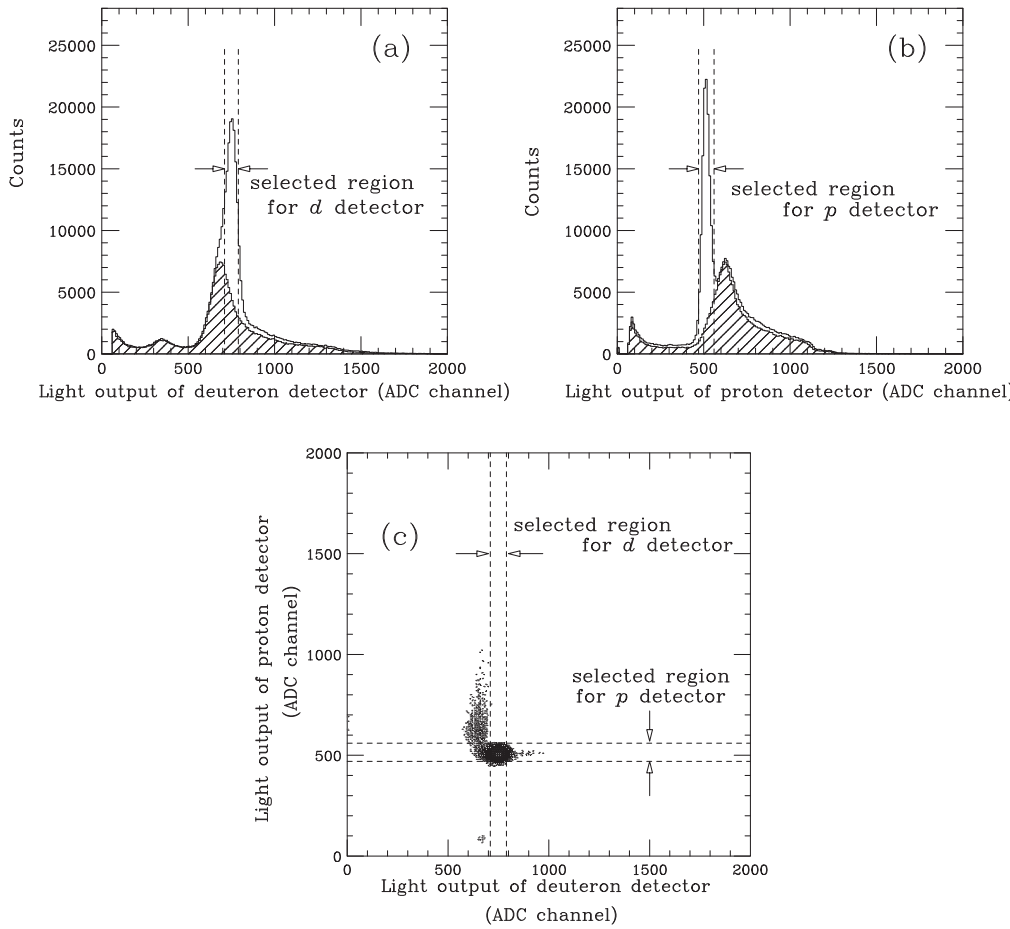

FIG. 3. Spectra of light outputs in the scintillation detectors for the scattered deuterons (a) and the recoil protons (b). The deuteron and proton detectors were placed at 25.1° and 43.0°, respectively. Hatched line region indicates accidental coincidence events estimated by coincidence triggering between adjacent beam bunches. After subtracting accidental coincidence events a two-dimensional plot of the deuteron and proton scintillator detector outputs was obtained (c).

beams were stopped in a Faraday cup placed at the focal plane F0 of the BigRIPS spectrometer (see Fig. 1).

III. DATA ANALYSIS AND EXPERIMENTAL RESULTS

Figures 3(a) and 3(b) show spectra of light outputs in the scintillation counters for the measurement performed at 294 MeV/nucleon. The scattered deuterons and recoil protons were detected at 25.1° and 43.0°, respectively. Accidental coincidence events estimated by coincidence triggering between adjacent beam bunches are indicated by the hatched lines in the spectra. Figure 3(c) shows a two-dimensional plot of the deuteron and proton scintillator detector outputs which was obtained after subtracting the accidental coincidence events. Identification of the scattered deuterons and recoil protons for dp elastic events was performed by cuts for the spectrum as shown in the Fig. 3(c). Selected region for each detector is also indicated in the Figs. 3(a) and 3(b).

The deuteron analyzing powers for elastic dp scattering are expressed through the unpolarized (σ_0) and polarized (σ) cross sections together with the vector and tensor polarizations of the incoming deuteron (p_Z and p_{ZZ}) as

$$\begin{aligned}\sigma = \sigma_0 \Big\{ & 1 + \sqrt{3}\, i T_{11}(\theta) p_Z \sin\beta \cos\phi \\ & + \frac{1}{\sqrt{8}} T_{20}(\theta) p_{ZZ} (3\cos^2\beta - 1) \\ & + \sqrt{3} T_{21}(\theta) p_{ZZ} \cos\beta \sin\beta \sin\phi \\ & - \frac{\sqrt{3}}{2} T_{22}(\theta) p_{ZZ} \sin^2\beta \cos 2\phi \Big\}, \end{aligned} \quad (1)$$

where θ and ϕ are the polar and azimuthal scattering angles, respectively [35]. The β is defined as the angle between the deuteron spin and beam direction. In this experiment the polarization axis of the deuteron beam was rotated with a Wien

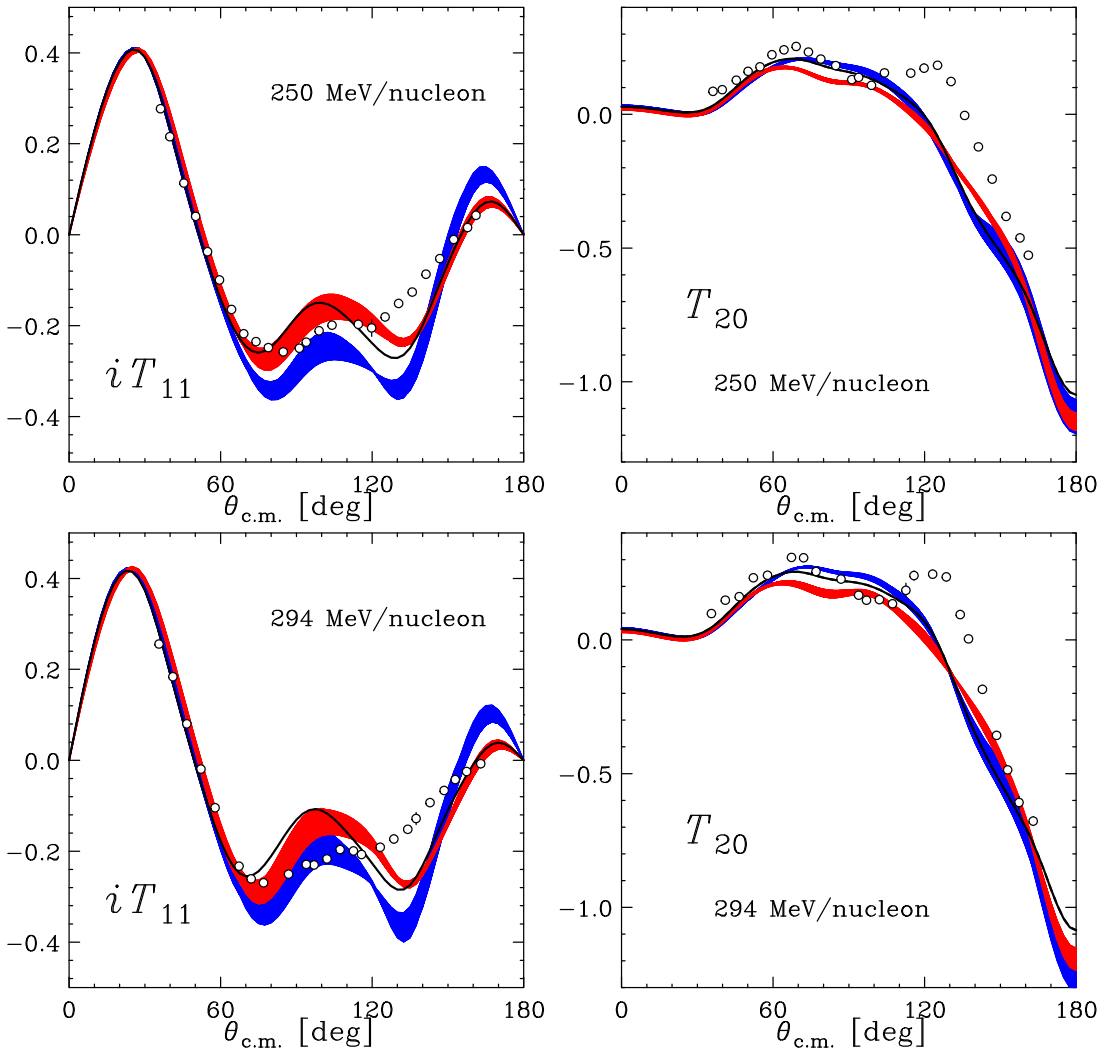

FIG. 4. (Color online) Deuteron analyzing powers iT_{11} and T_{20} for dp elastic scattering at 250 and 294 MeV/nucleon. The dark shaded (blue) bands contain predictions of modern NN potentials alone (AV18, CD Bonn, Nijmegen I and II). The light shaded (red) bands result when those potentials are combined with the TM99 3NF, properly adjusted to reproduce the ^{3}H binding energy. The solid curves show the result obtained with the combination AV18 + Urbana IX. The experimental data are shown with open circles.

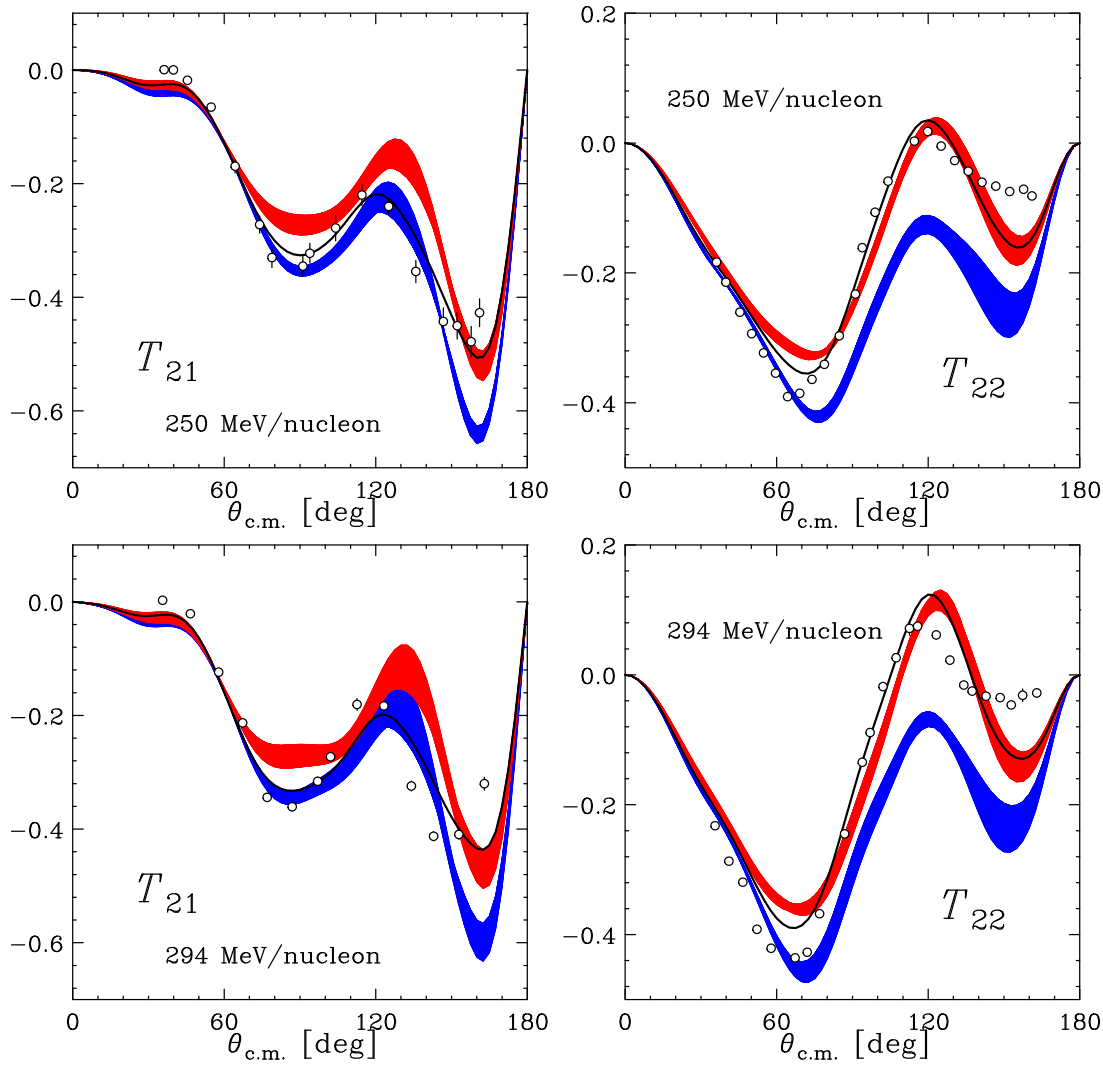

FIG. 5. (Color online) Deuteron analyzing powers T_{21} and T_{22} for dp elastic scattering at 250 and 294 MeV/nucleon. For description of bands and curves see Fig. 4.

filter system to the direction required for the measurement of a particular analyzing power [33]. For the measurement of the analyzing powers iT_{11}, T_{20}, and T_{22} the polarization axis was normal to the horizontal plane. For the T_{21} measurement the spin symmetry axis was rotated in the reaction plane and aligned at an angle β to the beam direction.

The experimental results for deuteron analyzing powers are shown as open circles in Figs. 4 and 5. In these figures only statistical uncertainties are shown. Their values are less than 0.02, 0.02, 0.03, and 0.01 for iT_{11}, T_{20}, T_{21}, and T_{22}, respectively. The uncertainty of the deuteron beam polarization is less than 3%.

The effects of the backgrounds other than accidental coincidence events, e.g., events of the proton knock-out reaction and those of the deuteron breakup reactions, were estimated by changing the selected region shown in Fig. 3(c). The integration range of a peak was changed systematically from the full width at 1/70 maximum to the full width at half maximum for the deuteron and proton detectors, respectively. The results of the analyzing powers changed by 0.004 or less. Therefore the uncertainties from the background events did not override the statistical ones.

IV. THEORETICAL FORMALISM AND DYNAMICAL INPUTS

Our standard nonrelativistic formulation of the Nd scattering with neutron and protons interacting through only a NN interaction v_{NN}, which is equivalent to the nonrelativistic three-nucleon Schrödinger equation plus boundary conditions, is described in terms of a breakup operator T satisfying the Faddeev-type integral equation [36,37]

$$T|\phi\rangle = tP|\phi\rangle + tPG_0T|\phi\rangle. \tag{2}$$

The two-nucleon (2N) t-matrix t is the solution of the Lippmann-Schwinger equation with the interaction v_{NN}. The permutation operator $P = P_{12}P_{23} + P_{13}P_{23}$ is given in terms of the transposition operators, P_{ij}, which interchange nucleons i and j. The incoming state $|\phi\rangle = |\mathbf{q}_0\rangle|\phi_d\rangle$ describes the free Nd motion with relative momentum $\mathbf{q}_0$ and the deuteron

state $|\phi_d\rangle$. Finally, G_0 is a resolvent of the three-body center of mass kinetic energy. Transition operator for the elastic Nd scattering U is given in terms of T by [36,37]

$$U = PG_0^{-1} + PT. \tag{3}$$

When in addition to pairwise interactions v_{NN} between three nucleons also a $3N$F is included, a new term V_4 appears in a potential energy of the $3N$ system

$$V_4 = V_4^{(1)} + V_4^{(2)} + V_4^{(3)}. \tag{4}$$

Each $V_4^{(i)}$ is symmetric under exchange of the nucleons j and k ($i,j,k = 1,2,3$ and $j \neq i \neq k$). In the 2π-exchange 3NF $V_4^{(1)}$ is a contribution to the $3N$ potential from (off-shell) rescattering of a pion on nucleon 1. Now on top of rescatterings among three nucleons induced by pairwise forces only, which are summed up in integral equation (2), additional rescatterings induced by $3N$F and NN interaction appear. Therefore Faddeev equation (2) has to be replaced by

$$\begin{aligned} T|\phi\rangle = {} & tP|\phi\rangle + (1+tG_0)V_4^{(1)}(1+P)|\phi\rangle \\ & + tPG_0\,T|\phi\rangle + (1+tG_0)V_4^{(1)}(1+P)\,G_0\,T|\phi\rangle, \end{aligned} \tag{5}$$

with one new contribution in the leading term and one in the kernel [37,38]. In the elastic scattering operator U two new contributions appear [37,38]:

$$U = PG_0^{-1} + V_4^{(1)}(1+P) + PT + V_4^{(1)}(1+P)G_0T. \tag{6}$$

The second term is due to a single interaction of three-nucleons via a $3N$F and the fourth results from rescatterings among three nucleons induced by two- and three-nucleon forces with a $3N$F as the final interaction.

The formal structure of these equations in the relativistic case remains the same but the ingredients change. As explained in Ref. [39] the relativistic three-nucleon rest Hamiltonian (mass operator) has the same form as the nonrelativistic one, only the momentum dependence of the kinetic energy and the relation of the pair interactions in the three-body system to the pair interactions in the two-body problem change.

The free relativistic invariant mass of three identical nucleons of mass m has the form [40]

$$M_0 = \sqrt{m_{230}^2 + q^2} + \sqrt{m^2 + q^2} \tag{7}$$

with a spectator momentum $\mathbf{q} = \mathbf{q}_1$ and the free two-body mass operator m_{230} expressed in terms of the relative momentum $\mathbf{k} = \mathbf{k}_{23}$ in the 2–3 total momentum zero frame

$$m_{230} \equiv 2\sqrt{k^2 + m^2} \equiv 2\omega_m(k). \tag{8}$$

As introduced in Ref. [41] the pair forces in the relativistic three-nucleon $2+1$ mass operator are related to the two-body forces in the two-body problem, v_{ij}, by

$$V_{(ij)(k)} = \sqrt{(m_{ij0} + v_{ij})^2 + q^2} - \sqrt{m_{ij0}^2 + q^2}, \tag{9}$$

where $V_{(ij)(k)}$ for $\mathbf{q} = 0$ reduces to the interaction v_{ij}, which acts in the two-body center of momentum frame.

The transition matrix t that appears in the Faddeev equation is obtained by solving the relativistic Lippmann-Schwinger equation as a function of q^2

$$t(\mathbf{k},\mathbf{k}';q^2) = V(\mathbf{k},\mathbf{k}';q^2) + \int d^3k'' \frac{V(\mathbf{k},\mathbf{k}'';q^2)t(\mathbf{k}'',\mathbf{k}';q^2)}{\sqrt{(2\omega_m(k'))^2 + q^2} - \sqrt{(2\omega_m(k''))^2 + q^2} + i\epsilon}. \tag{10}$$

The input two-body interaction V is computed by solving the nonlinear equation [42]

$$\left\{\sqrt{m_{ij0}^2 + q^2}, V_{(ij)(k)}\right\} + V_{(ij)(k)}^2 = 4mv_{NN}, \tag{11}$$

where v_{NN} is a nonrelativistic NN potential fitted to the NN data basis and where anticommutator $\{A,B\} \equiv AB + BA$. In case of $\mathbf{q} = \mathbf{0}$ that equation reduces to a nonlinear equation for the relativistic two-body interaction v. Therefore the problem of refitting all $2N$ data when changing from a nonrelativistic to a relativistic Lippmann-Schwinger equation is avoided. The nonlinear equation (11) can be solved by iterations [42].

The new relativistic ingredients in the Faddeev equation are therefore the t operator (10) (expressed in partial waves) and the resolvent of the $3N$ invariant mass

$$G_0 = \frac{1}{E + i\epsilon - M_0}, \tag{12}$$

with M_0 given by Eq. (7). E is the total $3N$ invariant mass expressed in terms of the initial neutron momentum $\mathbf{q}_0$ relative to the deuteron by

$$E = \sqrt{M_d^2 + q_0^2} + \sqrt{m^2 + q_0^2}, \tag{13}$$

with M_d the deuteron rest mass. Related to the choice of the permutation operator P the pair i-j is chosen as 2-3.

Currently, the Faddeev equation in its nonrelativistic or relativistic form is numerically solved for any NN interaction and $3N$F using a momentum space partial-wave decomposition. Details are presented in Refs. [30,36,37,43,44]. Projecting Eqs. (2) and (5) on such a basis turns it into a coupled set of two-dimensional integral equations. As shown in Refs. [30,40,45], in the relativistic case we can keep the same formal structure, though the permutation operators are replaced by the corresponding Racah coefficients for the Poincaré group, which include both Jacobians and Wigner rotations that do not appear in the nonrelativistic permutation operators [37,43].

In the nonrelativistic case the partial-wave projected momentum-space basis is

$$\left| pq(ls)j\left(\lambda\frac{1}{2}\right)IJ\left(t\frac{1}{2}\right)T\right\rangle, \tag{14}$$

where p and q are the magnitudes of standard Jacobi momenta (see Refs. [37,43]), $(ls)j$ are two-body quantum numbers with obvious meaning, $(\lambda 1/2)I$ refer to the third spectator nucleon, taken as the nucleon 1 and described by the momentum q, and J is the total three-nucleon angular momentum. Finally, t and T are the corresponding subsystem and total $3N$ isospin quantum numbers. In the relativistic case this basis is replaced by the Poincaré irreducible states defined in Refs. [30,40] and for which the short-hand notation $|k,q,\alpha\rangle$ is used:

$$\begin{aligned}|k,q,\alpha\rangle \equiv \left| kq(ls)j\left(\lambda,\frac{1}{2}\right)IJ\left(t\frac{1}{2}\right)T\right\rangle = |(J,q)\mathbf{P}\\ = \mathbf{0},\mu;\lambda,I,j_{23},k_{23},l_{23},s_{23}\rangle\left|\left(t\frac{1}{2}\right)T\right\rangle.\end{aligned} \tag{15}$$

Due to the short-range nature of the NN interaction it can be considered negligible beyond a certain value $j_{\max}$ of the total angular momentum in the $2N$ subsystem. Generally with increasing energy $j_{\max}$ will also increase. For $j > j_{\max}$ we set the t matrix to zero, which yields a finite number of coupled channels for each total angular momentum J and a total parity $\pi = (-)^{l+\lambda}$ of the $3N$ system. To achieve converged results at incoming nucleon laboratory energies below ≈300 MeV all partial wave states with the total angular momenta of the $2N$ subsystem up to $j_{\max} = 5$ and all total angular momenta of the $3N$ system up to $J = 25/2$ must be taken into account. Since the $3N$F is short-ranged its inclusion needs to be carried through only for all total angular momenta of the $3N$ system up to $J = 13/2$.

In our nonrelativistic calculations we applied standard, high-precision NN potentials (AV18 [1], CD Bonn [2], and Nijmegen I and Nijmegen II [3]) alone and combined with TM99 $3N$F [28]. The cutoff parameter Λ of that $3N$F was adjusted separately for each NN potential to give, together with that interaction, the experimental binding energy of ^{3}H. The AV18 potential was also combined with the Urbana IX $3N$F [29].

To study the importance of relativistic effects at investigated energies we generated solutions of relativistic $3N$ Faddeev equation with TM99 $3N$F included. Starting from the CD Bonn potential and solving nonlinear equation (11) at the required spectator nucleon momenta q, we produced the relativistic, on-shell equivalent interaction with boost effects incorporated exactly. That interaction served as a dynamical input to calculate, using the relativistic Lippmann-Schwinger equation (10), the relativistic off-shell t-matrix t that appears in the Faddeev equations.

Since in Ref. [40] it was found that effects of Wigner spin rotations are practically negligible in the studied energy range, we neglected them in the present study. When performing relativistic calculations with $3N$F included one requires matrix elements of the TM99 $3N$F in a relativistic momentum space basis $|k,q,\alpha\rangle$. In order to avoid calculations of the TM99 $3N$F matrix elements in that basis we assumed that the matrix elements in relativistic and nonrelativistic bases are equal:

$$\langle k,q,\alpha|V_4^{(1)}|k',q',\alpha'\rangle = \langle p = k,q,\alpha|V_4^{(1)}|p' = k',q',\alpha'\rangle. \tag{16}$$

That assumption allowed us to use the existing matrix elements of the TM99 $3N$F. It was checked in Ref. [30] that such an approximation is justified.

V. COMPARISON OF DATA WITH THEORETICAL PREDICTIONS

In Figs. 4 and 5 we compare measured deuteron analyzing powers with the theoretical predictions based on different dynamical inputs.

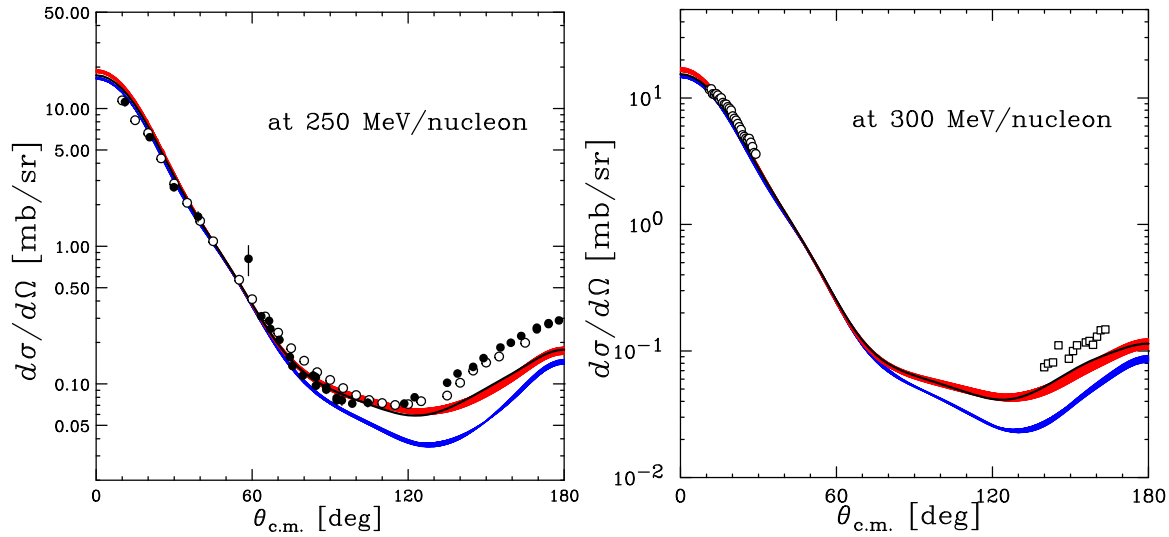

FIG. 6. (Color online) Cross section for 250 and 300 MeV/nucleon. The data shown at 250 MeV/nucleon are *pd* data (open circles) [18] and *nd* data (solid circles) [21]. The data shown at 300 MeV/nucleon are *pd* data at 295 MeV/nucleon (open circles) [47] and *pd* data at 316 MeV/nucleon (open squares) [48]. For description of bands and curves see Fig. 4.

The nonrelativistic theoretical predictions shown are based on modern NN forces alone and on their combinations with $3N$F models. We used high-precision NN potentials AV18 [1], CD Bonn [2], and Nijmegen I and II [3] alone [dark shaded (blue) bands in the figures] or combined them with the TM99 3NF [28] with the cutoff Λ properly adjusted [light shaded (red) bands in the figures]. In case of the AV18 potential, we also combined it with the Urbana IX $3N$F [29] (solid curves). In our calculations we neglected the Coulomb force acting between two protons. At energies considered here its effect on polarization observables is small [46].

For the vector analyzing power iT_{11} the predicted $3N$F effects are large for c.m. angles $\theta_{\text{c.m.}} \gtrsim 80^\circ$ both at 250 and 294 MeV/nucleon. Discrepancies between data and theory based on NN forces only are also clearly seen in that angular range. However, only a part of these discrepancies are removed by adding 3NFs. For $\theta_{\text{c.m.}} \lesssim 60^\circ$ $3N$F effects are negligible and the data are reproduced by the pure NN force predictions.

For the tensor analyzing power T_{20}, the predicted $3N$F effects are moderate. Drastic discrepancies between theory and data in the angular region $\theta_{\text{c.m.}} \sim 110$–$160^\circ$ are clearly seen for both energies. They are not explained by adding the TM99 or Urbana IX $3N$Fs. For angles $\theta_{\text{c.m.}} \lesssim 100^\circ$ the data are reasonably well reproduced by the theoretical predictions with the Urbana IX $3N$F included.

The data for the tensor analyzing power T_{21} are reproduced quite well by calculations with the NN forces only for both incident energies and angles $\theta_{\text{c.m.}} \lesssim 90^\circ$. At larger angles they deviate from the data. Inclusion of the TM99 and Urbana IX $3N$Fs improves description of data at angles $\theta_{\text{c.m.}} \gtrsim 150^\circ$. The large effects of the TM99 $3N$F predicted at angles $80^\circ \lesssim \theta_{\text{c.m.}} \lesssim 150^\circ$ are not supported by the T_{21} data. They differ clearly in that region of angles from the smaller effects of the Urbana IX $3N$F which generally leads to a better description of that observable.

For the tensor analyzing power T_{22}, the predicted $3N$F effects are large and similar in magnitude for the TM99 and

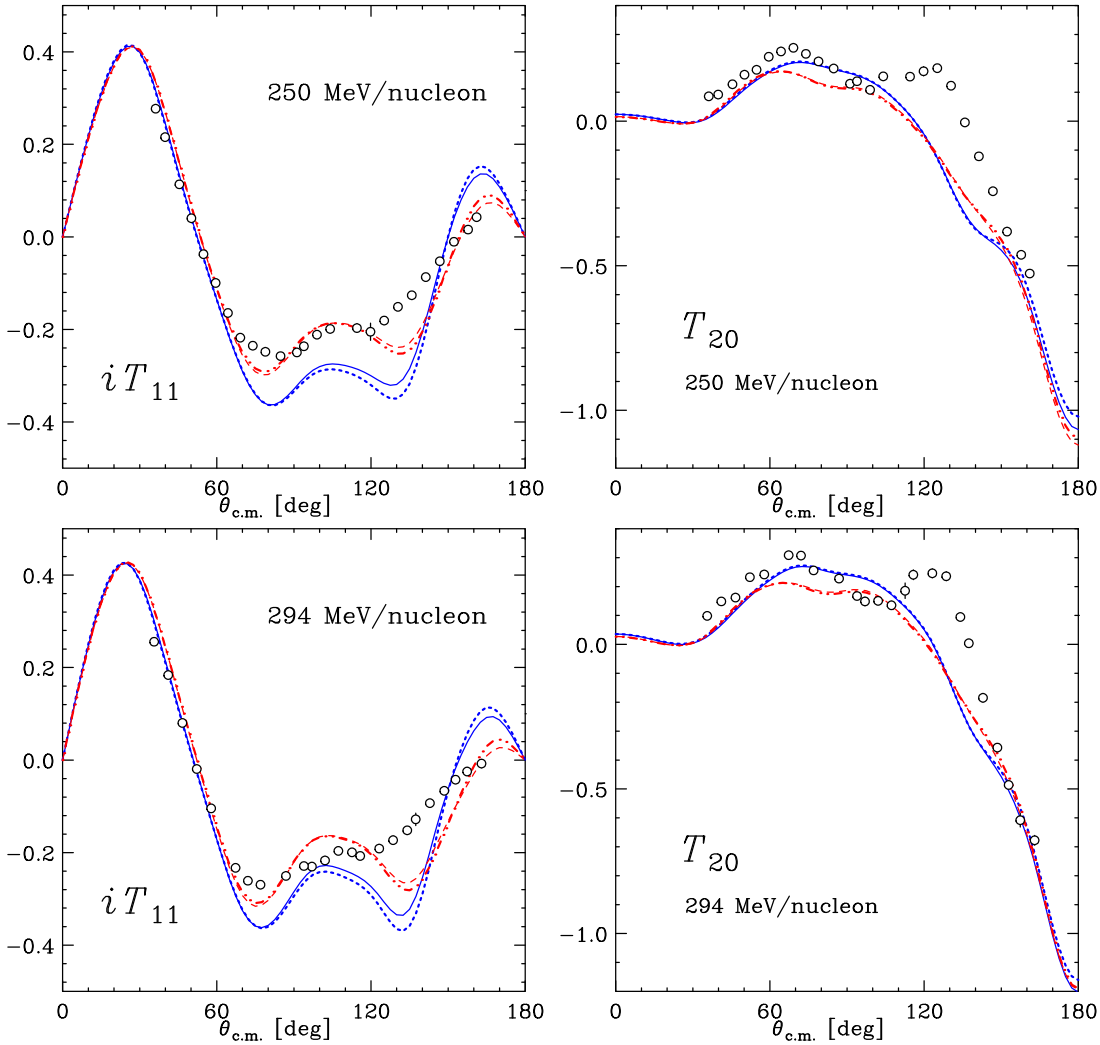

FIG. 7. (Color online) Deuteron analyzing powers iT_{11}, T_{20} for dp elastic scattering at 250 and 294 MeV/nucleon. The solid (blue) and dashed (red) curves show the results of nonrelativistic Faddeev calculations with the CD Bonn potential alone and combined with the TM99 $3N$F, respectively. The relativistic calculations based on the CD Bonn potential without Wigner spin rotations are shown with blue (dotted) curves. The red (double-dot-dashed) curves show the relativistic calculations with the TM99 $3N$F included.

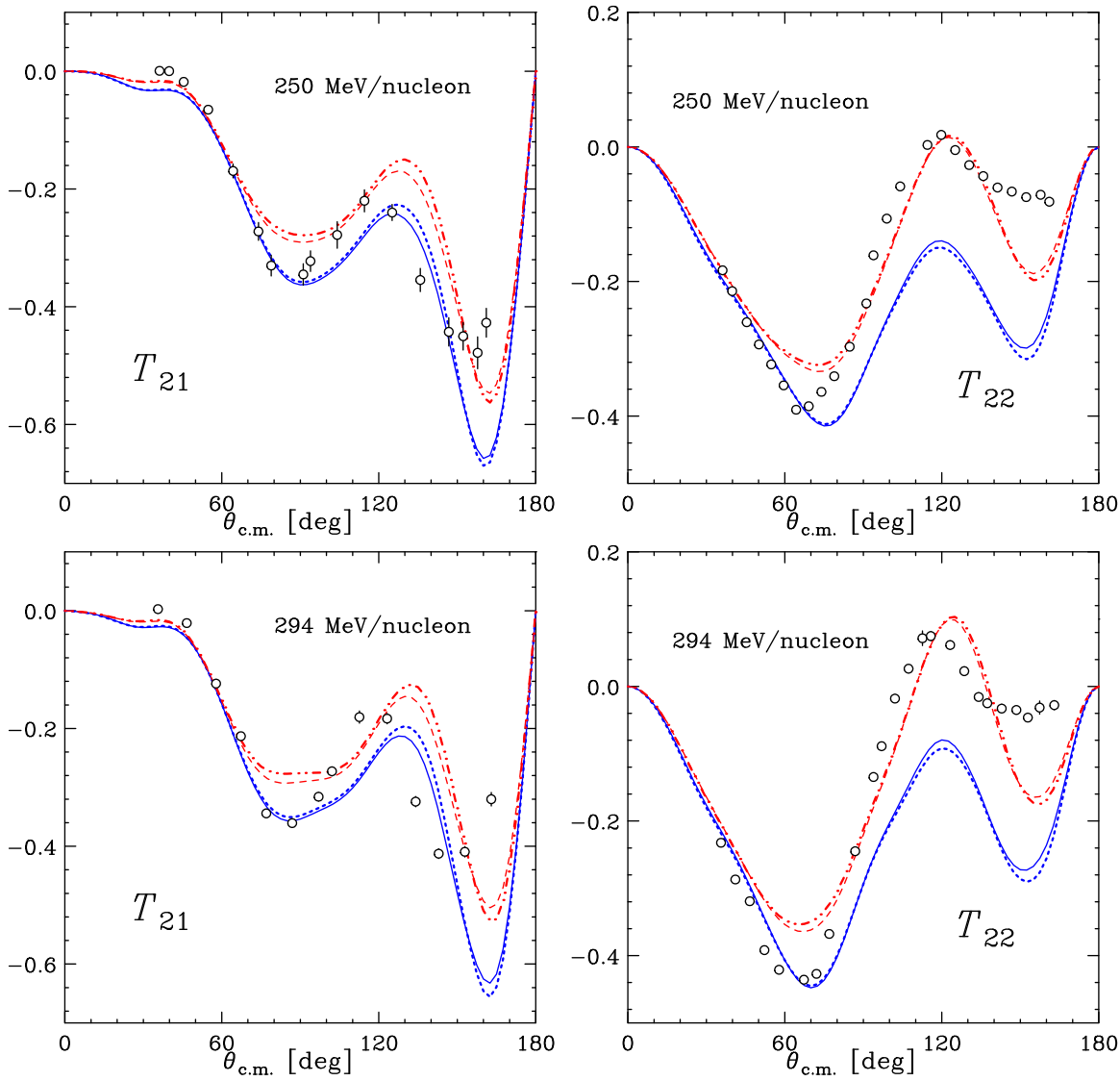

FIG. 8. (Color online) Deuteron analyzing powers T_{21} and T_{22} for dp elastic scattering at 250 and 294 MeV/nucleon. For description of curves see Fig. 7.

Urbana IX 3NFs. Large discrepancies between the data and predictions based on NN forces only are observed at angles $\theta_{\rm c.m.} \gtrsim 60^\circ$. The overall agreement is improved by taking into account TM99 and Urbana IX 3NFs except for the very backward angles $\theta_{\rm c.m.} \gtrsim 150^\circ$.

Generally the comparison of theory to data at 294 MeV/nucleon and 250 MeV/nucleon provides a consistent picture. All the deuteron analyzing powers at these two energies reveal around c.m. angles $\theta_{\rm c.m.} \gtrsim 120^\circ$ large discrepancies to theory based on NN forces alone. These discrepancies are not resolved completely by inclusion of the 3NFs. The 3NF effects at forward angles are small and the data at the forward angles are well described by the calculations with NN forces only. It should be noted that a similar pattern of discrepancies is obtained for the cross section. In Fig. 6 the elastic scattering cross-section data reported in Refs. [18,21,47,48] are compared with the theoretical predictions based on NN potentials with and without the 3NF models. For c.m. angles $\theta_{\rm c.m.} \gtrsim 120^\circ$ large discrepancies to theory are left even when the TM99 or Urbana IX 3NFs are included.

The discrepancies between data and theory found at 250 and 294 MeV/nucleon indicate that some significant dynamical component is missing in the calculations, especially in the regions of higher momentum transfer. Since our energies are large and since we use a nonrelativistic formulation, before looking for a possible candidate to explain the above discrepancies, one needs to find out the magnitude of relativistic effects. In Figs. 7 and 8 we show our data compared to the nonrelativistic and relativistic predictions based on the CD Bonn potential with and without taking the TM99 3NF into account. Comparing in both cases nonrelativistic and relativistic predictions leads to a conclusion that relativistic effects, if 3NF is acting or not, are small and only slightly alter the deuteron analyzing powers. For the cross section the relativistic effects are restricted mostly to very backward angles $\theta_{\rm c.m.} \gtrsim 160^\circ$ where they slightly increase the cross

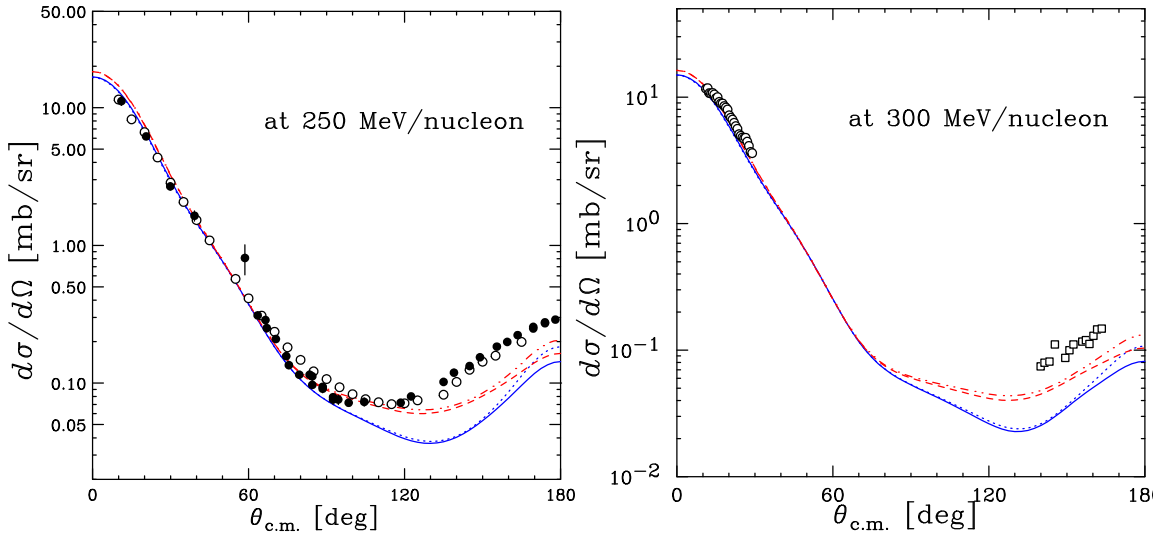

FIG. 9. (Color online) Cross section for 250 and 300 MeV/nucleon. For description of curves see Fig. 7.

section. That increase is, however, too small to explain the large discrepancy between data and theory found in Fig. 6 (see Fig. 9).

The smallness of relativistic effects strongly supports the conclusion that important components of the 3*N*F are missing in our calculations. In the meson exchange picture, contributions of heavy meson exchanges, e.g., π-ρ and ρ-ρ exchanges, would provide shorter range components of a 3*N*F. Such components appear also in χEFT, where already the leading nonvanishing 3*N*F starts at next-to-next-to-leading (NNLO) order of chiral expansion and consists of 2π-exchange, 1π-exchange-contact, and 3*N*-contact interaction topologies [49]. At the higher order (NNNLO) additional short- and long-range components appear with different momentum-spin dependencies [50,51]. With increasing energy these short-range terms are expected to become more important. The discrepancies between data and theory found for the deuteron analyzing powers show a complicated pattern of energy and angular dependence. This, together with the strong dependence of theoretical predictions on the 3*N*F model used, indicates the importance of such short-range components for the full description of these observables.

VI. SUMMARY AND CONCLUSIONS

We have reported a complete set of high-precision data for the deuteron analyzing powers iT_{11}, T_{20}, T_{21}, and T_{22}, in elastic dp scattering at 250 and 294 MeV/nucleon, taken in a wide angular range $\theta_{\text{c.m.}} = 35$–$163^\circ$. For all deuteron analyzing powers the statistical uncertainties are less than 0.03 and the systematic uncertainties do not exceed the statistical ones. These data constitute a solid basis to guide theoretical investigations of 3*N*F models at intermediate energies.

Our new deuteron analyzing power data together with elastic scattering cross-section data in the energy region of interest are compared with the results of three-nucleon Faddeev calculations based on modern *NN* potentials alone or combined with two commonly used models of 3*N*Fs, the Tucson-Melbourne 99 and Urbana IX. Large discrepancies between pure *NN* theory and data, which are not resolved by the current 3*N*Fs, were found at c.m. backward angles $\theta_{\text{c.m.}} \gtrsim 120^\circ$ for all the deuteron analyzing powers and the cross section. They indicate that significant dynamical components are missing in the region of higher momentum transfer. In order to estimate magnitude of relativistic effects we performed relativistic Faddeev calculations based on the CD Bonn potential with the TM99 3NF included or omitted. Small relativistic effects found for the deuteron analyzing powers and the cross section support the conclusion that short-range components of the 3*N*F, which are missing in our calculations and whose importance increases with increasing incident nucleon energy, are very probably responsible for the discrepancies between data and theory. To improve the description of the data at our energies, short-range 3NF components such as provided by χEFT should be applied. So far the framework of χEFT is only applicable up to $\sim$100 MeV/nucleon for 3*N* scattering. It will be interesting to see in the future how converged theoretical predictions based on χEFT forces describe our data.

ACKNOWLEDGMENTS

This experiment was performed at RI Beam Factory operated by RIKEN Nishina Center and CNS, University of Tokyo. This work was supported financially in part by the Grants-in-Aid for Scientific Research No. 20684010 and No. 24684013 of the Ministry of Education, Culture, Sports, Science, and Technology of Japan. It was also partially supported by the Polish National Science Center under Grant No. DEC2011/011B/ST2/00578, by the Japan Society for Promotion of Science (JSPS ID No. S-12028), and by the European Community-Research Infrastructure Integrating Activity "Exciting Physics of Strong Interactions" (acronym WP4 EPOS) under the Seventh Framework Program of EU. The numerical calculations were performed on the supercomputer cluster of the JSC, Jülich, Germany.

[1] R. B. Wiringa, V. G. J. Stoks, and R. Schiavilla, Phys. Rev. C **51**, 38 (1995).
[2] R. Machleidt, Phys. Rev. C **63**, 024001 (2001).
[3] V. G. J. Stoks, R. A. M. Klomp, C. P. F. Terheggen, and J. J. de Swart, Phys. Rev. C **49**, 2950 (1994).
[4] C. R. Chen, G. L. Payne, J. L. Friar, and B. F. Gibson, Phys. Rev. C **33**, 1740 (1986).
[5] T. Sasakawa and S. Ishikawa, Few-Body Syst. **1**, 3 (1986).
[6] A. Nogga, H. Kamada, W. Glöckle, and B. R. Barrett, Phys. Rev. C **65**, 054003 (2002).
[7] S. C. Pieper, V. R. Pandharipande, R. B. Wiringa, and J. Carlson, Phys. Rev. C **64**, 014001 (2001).
[8] P. Navrátil and W. E. Ormand, Phys. Rev. C **68**, 034305 (2003).
[9] See, e.g., A. Akmal *et al.*, Phys. Rev. C **58**, 1804 (1998).
[10] E. Epelbaum, A. Nogga, W. Glöckle, H. Kamada, Ulf-G. Meißner, and H. Witała, Phys. Rev. C **66**, 064001 (2002).
[11] S. Binder, J. Langhammer, A. Calci, P. Navrátil, and R. Roth, Phys. Rev. C **87**, 021303 (2013).
[12] T. A. Lähde *et al.*, Phys. Lett. B **732**, 110 (2014).
[13] K. Hebeler, S. K. Bogner, R. J. Furnstahl, A. Nogga, and A. Schwenk, Phys. Rev. C **83**, 031301 (2011).
[14] H. Witała, W. Glöckle, D. Hüber, J. Golak, and H. Kamada, Phys. Rev. Lett. **81**, 1183 (1998).
[15] N. Sakamoto *et al.*, Phys. Lett. B **367**, 60 (1996).
[16] H. Sakai *et al.*, Phys. Rev. Lett. **84**, 5288 (2000).
[17] K. Sekiguchi *et al.*, Phys. Rev. C **65**, 034003 (2002).
[18] K. Hatanaka *et al.*, Phys. Rev. C **66**, 044002 (2002).
[19] K. Ermisch *et al.*, Phys. Rev. C **71**, 064004 (2005).
[20] K. Sekiguchi *et al.*, Phys. Rev. Lett. **95**, 162301 (2005).
[21] Y. Maeda *et al.*, Phys. Rev. C **76**, 014004 (2007).
[22] E. J. Stephenson, H. Witała, W. Glöckle, H. Kamada, and A. Nogga, Phys. Rev. C **60**, 061001 (1999).
[23] R. Bieber *et al.*, Phys. Rev. Lett. **84**, 606 (2000).
[24] B. V. Przewoski *et al.*, Phys. Rev. C **74**, 064003 (2006).
[25] K. Sekiguchi *et al.*, Phys. Rev. C **70**, 014001 (2004).
[26] H. R. Amir-Ahmadi *et al.*, Phys. Rev. C **75**, 041001 (2007).
[27] K. Sekiguchi *et al.*, Phys. Rev. C **83**, 061001(R) (2011).
[28] S. A. Coon and H. K. Han, Few-Body Syst. **30**, 131 (2001).
[29] B. S. Pudliner, V. R. Pandharipande, J. Carlson, S. C. Pieper, and R. B. Wiringa, Phys. Rev. C **56**, 1720 (1997).
[30] H. Witała, J. Golak, R. Skibiński, W. Glöckle, H. Kamada, and W. N. Polyzou, Phys. Rev. C **83**, 044001 (2011).
[31] H. Okamura *et al.*, AIP Conf. Proc. **293**, 84 (1994).
[32] Y. Watanabe *et al.*, RIKEN Accel. Prog. Rep. **42**, 111 (2009).
[33] H. Okamura *et al.*, AIP Conf. Proc. **343**, 123 (1995).
[34] H. Mardanpour *et al.*, Eur. Phys. J. A **31**, 383 (2007).
[35] G. G. Ohlsen, Rep. Prog. Phys. **35**, 717 (1972).
[36] H. Witała, T. Cornelius, and W. Glöckle, Few-Body Syst. **3**, 123 (1988).
[37] W. Glöckle *et al.*, Phys. Rep. **274**, 107 (1996).
[38] D. Hüber *et al.*, Acta Phys. Polonica B **28**, 1677 (1997).
[39] W. Glöckle, T.-S. H. Lee, and F. Coester, Phys. Rev. C **33**, 709 (1986).
[40] H. Witała, J. Golak, R. Skibiński, W. Glöckle, W. N. Polyzou, and H. Kamada, Phys. Rev. C **77**, 034004 (2008).
[41] F. Coester, Helv. Phys. Acta **38**, 7 (1965).
[42] H. Kamada and W. Glöckle, Phys. Lett. B **655**, 119 (2007).
[43] W. Glöckle, *The Quantum Mechanical Few-Body Problem* (Springer-Verlag, Berlin and Heidelberg, 1983).
[44] D. Hüber, H. Witała, and W. Glöckle, Few-Body Syst. **14**, 171 (1993).
[45] H. Witała, J. Golak, W. Glöckle, and H. Kamada, Phys. Rev. C **71**, 054001 (2005).
[46] A. Deltuva, A. C. Fonseca, and P. U. Sauer, Phys. Rev. C **72**, 054004 (2005).
[47] H. Rohdjeß *et al.*, Phys. Rev. C **57**, 2111 (1998).
[48] J. C. Alder *et al.*, Phys. Rev. C **6**, 2010 (1972).
[49] E. Epelbaum, Prog. Part. Nucl. Phys. **57**, 654 (2006).
[50] V. Bernard, E. Epelbaum, H. Krebs, and Ulf-G. Meißner, Phys. Rev. C **77**, 064004 (2008).
[51] V. Bernard, E. Epelbaum, H. Krebs, and Ulf-G. Meißner, Phys. Rev. C **84**, 054001 (2011).